High-Resolution Infrared Spectroscopy of HCN−Zn_n ($n = 1-4$) Clusters: Structure Determination and Comparisons with Theory

Paul L. Stiles* and Roger E. Miller†

Department of Chemistry, University of North Carolina, Chapel Hill, North Carolina 27599

Received: January 3, 2006; In Final Form: March 7, 2006

High-resolution infrared laser spectroscopy has been used to obtain rotationally resolved spectra of HCN−Zn_n ($n = 1-4$) complexes formed in helium nanodroplets. In the present study the droplets passed through a metal oven, where the zinc vapor pressure was adjusted until one or more atoms were captured by the droplets. A second pickup cell was then used to dope the droplets with a single HCN molecule. Rotationally resolved infrared spectra are obtained for all of these complexes, providing valuable information concerning their structures. Stark spectra are reported and used to determine the corresponding permanent electric dipole moments. Ab initio calculations are also reported for these complexes for comparison with the experimental results.

Introduction

The main driving force for the study of metal clusters has been the detailed characterization of the transition in bonding that takes place as a cluster increases in size. This change in binding is especially relevant in the divalent groups of metals, where the smallest clusters are dominated by van der Waals forces, the intermediate cluster sizes by covalent bonds, and the bulk by metallic bonds. One of the benchmarks for such studies is that of the group 12 Hg_n clusters, for which there is considerable experimental and theoretical[1−5] literature. The isovalent Cd_n clusters have also been studied,[6,7] although to a somewhat lesser degree, while there is very little theoretical work[8−10] and virtually no experimental data on the Zn_n clusters.[11] In this series of divalent group 12 atoms, theory predicts that the transitions from van der Waals to covalent to metallic bonding will occur at progressively smaller sizes for the lighter atoms.[8] Thus, zinc atoms seem like prime targets for studying these transitions in a size range that is amenable to study with high-resolution spectroscopy methods.

In this paper, we present the experimental structural determinations for clusters containing multiple zinc atoms. The zinc clusters are formed in helium nanodroplets at 0.37 K, after which a single HCN molecule is added to make a metal cluster−adsorbate complex. These experiments were undertaken in a manner similar to that used in a previous study of HCN−Mg_n,[12] in which we showed that the magnesium clusters, ranging from two to six atoms in size, could be formed and their overall structure left relatively unperturbed by the addition of a single HCN molecule.

The use of helium droplets as an ultracold spectroscopic medium has been thoroughly demonstrated, and it is well-known that molecular complexes can freely rotate within the superfluid helium matrix,[13,14] allowing for the measurement of vibrational spectra with full rotational resolution. This free rotation is particularly useful in the study of metal cluster−adsorbate complexes. For example, in our previous HCN−Mg_n study,[12] the symmetry of the rovibrational spectrum of the C−H stretch gave direct insight into the overall symmetry of the complex. Although this symmetry within the droplet remains unaffected, a small fraction of the helium solvent rotates along with the complex, resulting in a slight increase in the measured moment of inertia. The quantification of this fraction has proven to be very difficult, and aside from a few model systems,[15−18] the determination of bond lengths via rovibrational spectroscopy remains beyond the current state of the art. Empirically, it has been found that heavy rotors[18] have rotational constants reduced by a factor of 2.5 ± 0.5 in helium when compared to their corresponding gas-phase values. This factor of 2.5 will be referred to throughout this paper when comparing ab initio/gas-phase rotational constants to those measured in helium droplets.

In addition to structural information, infrared spectroscopy can provide information on the nature of the interaction between the metal cluster and the adsorbate. For instance, the C−H stretching frequency in HCN was found to be very sensitive to the changing magnesium cluster size.[12] Specifically, we observed a dramatic vibrational red-shift for the HCN−$Mg_{n\geq 4}$, when compared to the HCN−$Mg_{n\leq 3}$. This shift pointed to a fundamental change in bonding between the HCN and magnesium cluster when going from HCN−Mg_3 to HCN−Mg_4 and was characterized by the measurement of each complex's dipole moment with Stark spectroscopy. The dipole moments of the $n \leq 3$ complexes were small and only slightly larger than the dipole moment of HCN, indicating a weak dipole induced dipole interaction. On the other hand, the dipole moment of HCN−Mg_4 was found to be 8.5 D, which is more than double the dipole moment of HCN. Through the use of charge density calculations it was found that HCN donated 0.15 electrons to the Mg_4 cluster, thus accounting for the very large dipole moment.

In the previous HCN−Mg_n study, we performed very high level ab initio calculations on the various metal cluster−adsorbate complexes. This investigation was simplified by the fact that magnesium is quasi-closed shell and has relatively few electrons, which is presumably why such a large volume of theoretical literature exists[19,20] with which to compare our

* Corresponding author. Phone: (919) 962-1579. Fax (919) 843-6041. E-mail: pstiles@email.unc.edu.
† Deceased.

10.1021/jp060042v CCC: $33.50
Published on Web 04/01/2006

calculations. The situation with the zinc clusters, however, is quite different because, as noted above, there exists little theoretical data on the small zinc clusters and no data on small zinc cluster's interactions with adsorbates. With very little work to compare our calculations to, the appropriate method had to be chosen with great care. Using the density functional methods of Wang et al.[10] seemed an unlikely candidate due to the poor performance of DFT when calculating weakly bound structures. Indeed, Zhao comments on the poor agreement between his calculations on Zn_2-Zn_4 when compared to the coupled cluster calculations of Flad[8] and Yu[9] and only includes these results to compare their overall bonding patterns to the higher order clusters. The HCN−Zn_n clusters reported here involved this very same weakly bound cluster size regime in addition to another weak bond between the cluster and the HCN molecule. We attempted the CCSD(T) methods of Flad and Yu but quickly found it to be unfavorable due to the large computational cost of such calculations. In the end we decided to approach the HCN−Zn_n cluster calculations with MP2 methods along with the use of relativistic effective core potentials (ECP), which will be discussed further below.

The large number of electrons associated with zinc atoms make all electron calculations very time-consuming. The standard method for reducing the computational cost of systems that contain large numbers of electrons is to replace the core electrons that do not actively participate in bonding with a potential. This potential mimics the behavior of the innermost electrons while drastically cutting the amount of basis functions required for electronic structure calculations. An important advantage that accompanies the use of an ECP is the ability to include scalar and spin−orbit relativistic effects within the potential itself,[21] which becomes increasingly important as the mass of the atom increases. The primary disadvantage is the omission of core polarization, which becomes important when calculating the geometries of van der Waals type complexes.[8] In the case of zinc clusters, this disadvantage can be minimized by using a "small-core ECP", which replaces the inner 10 electrons, as opposed to using a "large-core ECP", which replaces 28 of the 30 electrons.[22] Alternatively, a core polarization potential (CPP) can be added to the large-core ECP. The CPP reproduces the core−valence correlation on the valence electrons and has the tendency to contract the valence electrons.[23] CPPs are available in Molpro[24] but not in the Gaussian[25] ab initio package.

Computational Details

Gaussian 2003[25] was used for all calculations presented in this paper. Geometry optimizations were set with the tight convergence settings. The approach taken here was guided by previous zinc cluster studies [8,9,26]and recommendations taken from an earlier study based upon ECPs.[27] In the end, we chose to use the ECP10MDF small-core ECP, with an accompanying (8s7p6d)→[6s5p3d] valence basis set, which was further augmented with 2f and 1g functions.[27] The HCN was treated using a 6-311++G(d,p) basis set.

In an effort to benchmark the present calculations against those of previous studies, we began by carrying out calculations for neat zinc complexes. Table 1 summarizes the results of these calculations, along with those from earlier studies by Flad et al.[8,28] Although we omitted the core polarization potential and have used a slightly smaller basis set, the agreement is quite reasonable. Indeed, our MP2 and CCSD(T) calculations show the same trends in bond lengths with cluster size. Notice the large contraction in bond length when going from Zn_3 to Zn_4.

TABLE 1: Bond Lengths (Å) for the Zinc Dimer, Trimer, and Tetramer, Calculated at the MP2 and CCSD(T) Level, Using the Stuttgart−Dresden ECP10MDF Effective Core Potential and the (8s7p6d2fg)→[6s5p3d2fg] Valence Basis Set[a]

	MP2	CCSD(T)	small-core ECP/CCSD(T)	large-core ECP/CCSD(T)
Zn_2	3.8291	4.1927	3.959	4.150
Zn_3	3.3896	3.9508		3.75
Zn_4	2.7080	2.9358		2.94

[a] These are compared to previous CCSD(T) calculations using the same small-core ECP,[8] in addition to calculations using the large-core ECP28MWB potential.[28] The difference between the two small-core CCSD(T) calculations is due to our omission of a counterpoise correction in the geometry optimization and the use of a slightly smaller valence basis set.

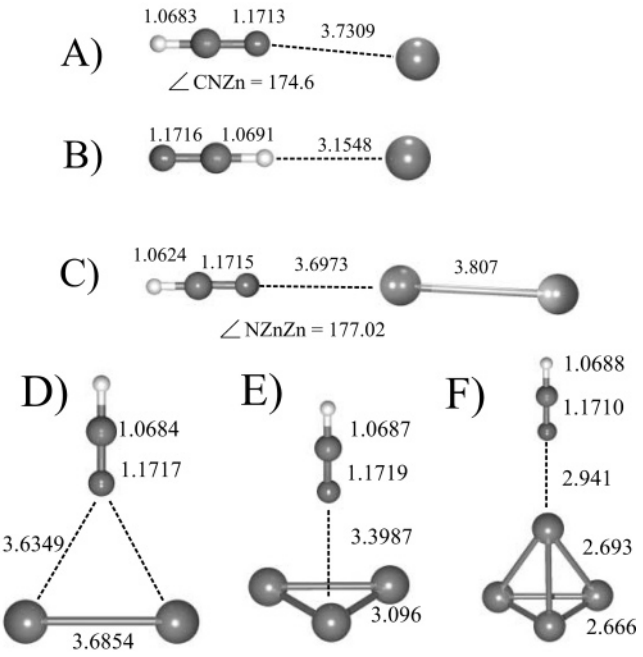

Figure 1. Calculated minimum energy structures and relevant bond lengths for the various HCN−Zn_n ($n = 1-4$) complexes, using the ECP10MDF ECP and MP2 level of theory: (A) HCN−Zn, (B) hydrogen-bound linear Zn−HCN, (C) near-linear HCN−Zn_2, (D) T-shaped HCN−Zn_2, (E) C_{3v} HCN−Zn_3, and (F) C_{3v} HCN−Zn_4. The bond lengths are given in angstroms. The HCN−Zn_2 T-shaped structure contains one imaginary frequency upon vibrational analysis.

This increase in stabilization for Zn_4 is analogous to those seen in the magnesium clusters and will be addressed later in this paper.

Ab initio calculations for HCN−Zn_n ($n = 1-4$) were carried out at the MP2 level, the results of which are summarized in Figure 1 and Table 2. The CCSD(T) calculations were simply too expensive for the adsorbate−metal cluster systems. Fortunately, the comparisons for the naked metal clusters suggest that the structures obtained at the MP2 level are reasonable, although the zinc interatomic bond lengths were systematically smaller than those obtained from the CCSD(T) calculations. Harmonic frequencies were also calculated at the MP2 level for these HCN−Zn_n complexes. No imaginary frequencies were obtained at the optimized geometries reported in Figure 1. However, it should be noted that experimental data, to be presented below, strongly suggest that the HCN−Zn_2 complex is T-shaped, a structure that ECP/MP2 theory predicts as a first-order transition state. Table 2 summarizes the vibration frequency shifts (from the HCN monomer) for the C−H stretching mode, along with the ab initio values for the permanent electric

TABLE 2: Comparison of the Calculated and Experimental Vibrational Frequency Shifts (all to the red) of the C−H Stretches (from the HCN monomer)[a]

	MP2		experiment	
	$\Delta\nu$ (cm^{-1})	μ (D)	$\Delta\nu$ (cm^{-1})	μ (D)
HCN−Zn	2.05	3.51	1.3	3.20 ± 0.05
Zn−HCN	20.4	3.44	30.2	−
(L) HCN−Zn_2	2.46	3.74	2.53	3.7 ± 0.5
(T) HCN−Zn_2	4.19	3.71		
HCN−Zn_3	7.17	3.97	4.33	3.85 ± 0.05
HCN−Zn_4	7.80	5.34	7.60	−

[a] The calculated and experimental dipole moments are also given. The excited and ground-state dipole moments were set to equal during the fit to the Stark spectra. The MP2 calculations used the same valence basis set and ECP that was used for the bare zinc clusters. The two entries for HCN−Zn_2 correspond to the linear (L) and T-shaped (T) structures. (Frequency calculations of the T-shaped structure contain one imaginary vibration.)

TABLE 3: A Summary of the Experimentally Determined Rotational Constants (cm^{-1}) Determined in the Ground and Vibrationally Excited State[a]

Experiment

rotational constants (cm^{-1})	HCN−Zn	Zn−HCN	HCN−Zn_2	HCN−Zn_3	HCN−Zn_4
A	−	−	0.019	0.0108	0.005
B''	0.0236	0.004	0.015	0.0107	0.00490
B'	0.0238	0.004	0.015	0.0106	0.00488
C''	−	−	0.0091	0.0107	0.00490
C'	−	−	0.0092	0.0106	0.00488
D''	1.3×10^{-5}	−	−	5.3×10^{-6}	3×10^{-7}
D'	1.7×10^{-5}	−	−	5.2×10^{-6}	3×10^{-7}

MP2

rotational constants (cm^{-1})	HCN−Zn	Zn−HCN	HCN-Zn_2 linear	HCN-Zn_2 T-shaped	HCN−Zn_3	HCN−Zn_4
A	−	−	−	0.05217	0.02776	0.03710
B	0.04545	0.03766	0.01265	0.03883	0.02776	0.01487
C	−	−	−	0.02226	0.02751	0.01487

[a] The A rotational constant is given as the average between the ground and vibrationally excited states. The MP2 "gas-phase" rotational constants are also given. The calculated rotational constants for both the linear and T-shaped HCN−Zn_2 complexes are given, even though the later was calculated to be a transition state and the former did not agree with the experiment.

dipole moments. The calculated rotational constants are summarized in Table 3.

Experimental Method

The apparatus used in the present study has been discussed in detail previously.[29−31] The droplets are formed by expanding ultrapure helium through a 5 μm diameter nozzle, cooled by a closed-cycle helium refrigerator. The nozzle was operated at a pressure of approximately 60 bar and temperatures between 21.5 and 17 K, corresponding to mean droplet sizes of 1000 and 8000 atoms, respectively.[32,33] Zinc atoms were doped into the droplets by passing the latter through a 1.3 cm long oven, operated at a range of temperatures near 280 °C, monitored using a J-type thermocouple ($\approx 10^{-5}$ mbar of zinc).[34] HCN was added downstream of the metal oven in a separate pickup cell, the pressure of which was optimized for the capture of a single molecule.

The seeded droplets then pass through a laser interaction region, where the C−H stretch of the HCN is excited by an F-center laser (Burleigh FCL-20), operating on crystal #3 (RbCl:Li). Subsequent vibrational relaxation to the helium droplet results in the evaporation of approximately 600 helium atoms. The resulting depletion of the droplet beam is then detected by a liquid helium cooled bolometer.[35] The laser is amplitude modulated and the corresponding bolometer signals are measured using phase sensitive detection methods. The details associated with tuning and calibrating the laser can be found elsewhere.[36]

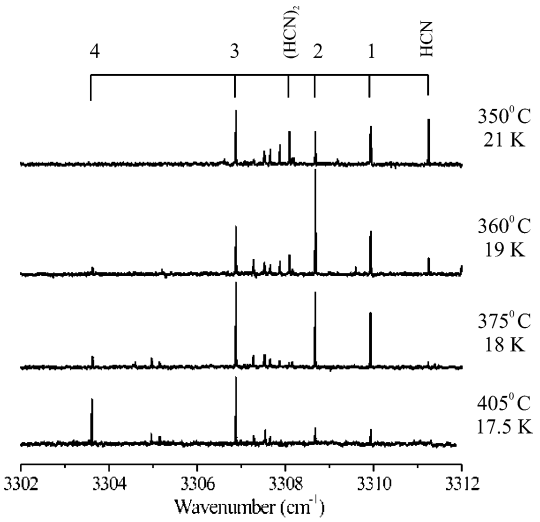

Figure 2. A series of pendular state spectra taken at various zinc oven temperatures and droplet sizes. HCN−Zn_n are labeled as well as the HCN and HCN dimer pendular peaks. The small, unlabeled peaks are due to higher order HCN clusters. The higher oven temperatures and larger droplets were required to form the larger clusters. The HCN pickup cell pressure was kept below the optimal pressure for the pickup of a single HCN molecule per droplet in order to decrease peak intensities arising from HCN multimers.

An electric field can also be applied to the laser interaction region, using two metal electrodes. A considerable enhancement of the signal levels is obtained by using a large electric field (~24 kV/cm) to collapse the entire rovibrational band into a single "pendular" peak.[37,38] The added sensitivity is particularly useful when searching for new species. At more modest electric fields (1−4 kV/cm), Stark spectra are recorded to obtain experimental dipole moments [39] for the HCN−Zn_n complexes.

Experimental Results

The experimental conditions required for the formation of the various HCN−zinc complexes were optimized by first adjusting the HCN pressure to achieve the best possible monomer signals. The zinc oven temperature was then slowly increased, while monitoring the HCN monomer signal.[40,41] The pickup of zinc atoms from the vapor resulted in a corresponding decrease in the HCN monomer signal, which was typically reduced by a factor of 2 before scanning was commenced. The initial search for the spectra corresponding to the C−H stretches of the HCN−Zn_n clusters was performed with a large dc electric field applied to the laser interaction region.

Figure 2 shows a series of pendular spectra, recorded over a range of zinc oven temperatures and helium droplet sizes. In particular, large droplets are required to form the larger zinc complexes, owing to the considerable condensation energy that is dissipated to the droplets. In the spectra shown in Figure 2, the HCN pickup cell pressure was deliberately kept below that required to optimize the HCN monomer signal to ensure that contributions from the HCN dimer, trimer, etc. were minimized,

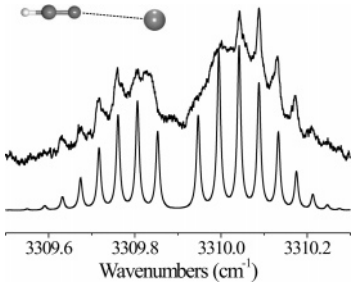

Figure 3. The full rotationally resolved spectrum of HCN−Zn. The simulated spectrum, plotted below the experimental spectrum, was generated with a linear rotor Hamiltonian (equilibrium structure is given in the inset).

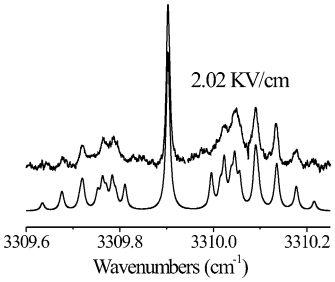

Figure 4. The fitted constants, along with the dipole moment, were used to fit the Stark spectrum. Diagonalizing the full Stark Hamiltonian generated the simulated Stark spectrum at 2.02 kV/cm (below experimental spectrum).

although these bands are still weakly visible. From the oven temperature dependence of the various peaks in these spectra (see Figure 2), we tentatively assign the peaks labeled $n = 1-4$ to the corresponding HCN−Zn_n complexes. In particular, the larger complexes are not seen at the lowest oven temperature (350° C), given that they require higher zinc vapor pressures and larger mean droplets size. The oven temperature and droplet size dependence of these bands is consistent with our previous observations of the corresponding magnesium clusters.[12] Indeed, the pattern of vibrational frequency shifts (from the HCN monomer) is also reminiscent of that observed for the HCN−Mg_n complexes.[12] Of particular note is the relatively large frequency shift in going from HCN−Zn_3 to HCN−Zn_4, which was also observed for the corresponding magnesium complexes. This behavior is quite different from that observed in van der Waals complexes[42] and is indicative of strongly nonadditive interactions. The tentative assignments given here can now be further tested by examining the individual bands in the absence of the strong dc electric field.

The Binary HCN−Zn Complex. Figure 3 shows a zero-field spectrum obtained in the region centered on the band labeled as 1 in the pendular spectrum shown in Figure 2. This spectrum is consistent with that of a linear molecule, showing well-resolved R and P branch transitions. A linear rotor fit to the experimental spectrum is shown in the Figure 3, from which the rotational constants and vibrational origin given in Table 3 are determined. As expected, the experimental rotational constant for the ground vibrational state (0.0236 cm^{-1}) is much smaller than the ab initio value for the binary complex (0.04545 cm^{-1}), corresponding to a ratio of 1.9, well within the range of values observed for a wide range of molecules in helium.[43] The small frequency shift of this band from the monomer suggests that the complex is nitrogen-bound, in agreement with the ab initio structure shown as an inset in Figure 3.

As is typical of helium solvated molecules, the low J transitions are rather broad compared to those associated with higher J states. This is consistent with the fact that low J states are more sensitive to the anisotropic interactions that might result from the surrounding solvent.[44−46] Unfortunately, due to the numerous broadening mechanisms, both homogeneous and inhomogeneous, the exact cause for the J-dependence of the line width is not completely understood.[47−52]

Figure 4 shows an experimental Stark spectrum of the HCN−Zn binary complex, recorded at an electric field of 2.02 kV/cm. A fit obtained by diagonalizing the full Stark Hamiltonian matrix[40] is shown below the experimental spectrum in Figure 4, based upon the rotational constants and band origin obtained from the zero-field spectrum. The Stark Hamiltonian matrix elements were generated using the asymmetric top basis set with J, K, and M up to 15, 12, and 15, respectively. The only adjustable parameter in this fit is the permanent electric dipole moment, which was assumed here to be the same in the ground and vibrationally excited states. As discussed in detail elsewhere,[53] the dipole moments determined by fitting a helium nanodroplet Stark spectrum require only minor corrections (1−2%) to account for the polarization of the solvent atoms. The dipole moment obtained from this analysis is 3.20 D, which is in reasonable agreement with the results from the ab initio calculations, namely 3.51 D. It should be pointed out that the latter value corresponds to the equilibrium structure of the HCN−Zn complex, while the experimental value includes the effects of vibrational averaging. As discussed previously for the HCN−Mg complex,[54] intermolecular bending of the complex results in an experimental dipole moment that is smaller than that for the equilibrium structure, which is in agreement with the difference observed here. These effects have also been discussed for a number of weakly bound van der Waals complexes.[55−57] The ab initio calculations give a binding energy for the HCN−zinc complex of only 116 cm^{-1} (uncorrected for zero-point energy), again suggesting that this system will undergo wide amplitude bending motion.

In the previous study of the HCN−Mg complex,[12 54] we showed that the increase in the dipole moment upon complex formation (the dipole moment of HCN is 2.979 D[58]) can be explained in terms of the polarizability of the metal atom. Not surprisingly, HCN−Zn behaves similarly. The ab initio dipole moment of HCN−Zn is somewhat smaller (3.51 D) than that of HCN−Mg (3.71 D), consistent with atomic polarizabilities of Zn and Mg, namely 7.1 and 10.6 $Å^3$, respectively.[34] In contrast, the experimental dipole moments for these two complexes are the same, within the experimental uncertainty, suggesting that the HCN−Zn complex is somewhat stiffer than HCN−Mg. This seems inconsistent with the fact that the ab initio HCN−Mg binding energy between the HCN and Mg atom is about 140 cm^{-1}, while that of HCN−Zn is about 120 cm^{-1}. However, considering the size of both metal atoms, one observes that the van der Waals radii for Zn and Mg are 1.39[59] and 1.73 Å,[59] respectively. This smaller size of zinc allows it to interact more closely with the lone pair on the nitrogen of HCN, thus reducing the amplitude of the bending motions and reducing the effects of vibrational averaging. It should also be pointed out that we neglected the core polarization in the calculations and therefore probably underestimated both the binding energy and induced dipole moment of the HCN−Zn complex. A high-level all-electron two-dimensional potential energy surface would be extremely helpful in the analysis of the vibrational averaging taking place in this complex, but at the moment, it is beyond the scope of this study.

Although the calculation of the full 2D intermolecular potential energy surface for the HCN−Zn complex has not been carried out, we concluded from a large number of geometry

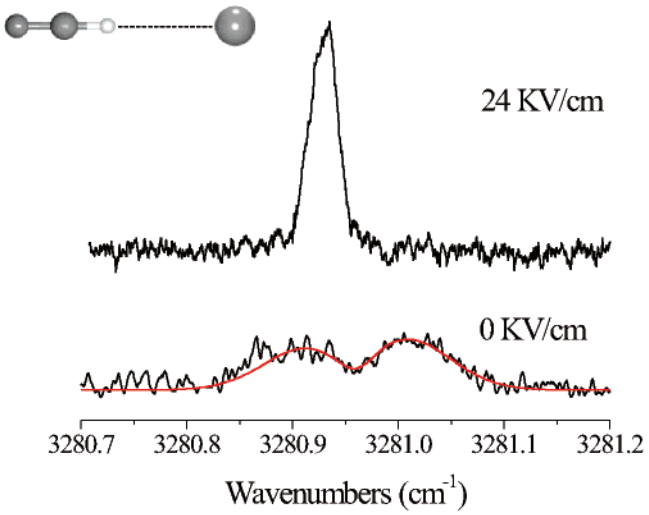

Figure 5. Pendular spectrum of the hydrogen-bound Zn−HCN complex (upper plot). The poorly resolved zero-field Zn−HCN spectrum (lower plot) is shown along with the crude fit. The calculated structure is shown in the inset.

optimizations that the nitrogen-bound complex discussed above corresponds to the global minimum on the ab initio surface. In addition to this complex, calculations revealed that a hydrogen-bound linear isomer exists in a local minimum on the surface. The corresponding geometry, vibrational frequency shift, and rotational constant are given in Figure 1 and Tables 2 and 3. Previous studies[60,61] have shown that the growth of complexes in helium nanodroplets (in the absence of strong dipole−dipole interactions) can result in the formation of these higher energy isomers. Owing to the hydrogen-bonded nature of this isomer, we expect that the corresponding spectrum will be more strongly shifted from the HCN monomer.

Figure 5 shows a pendular spectrum, along with the corresponding field-free spectrum, shifted from the HCN monomer by 30.2 cm^{-1}. This is to be compared with the ab initio frequency shift for the hydrogen-bonded Zn−HCN complex of 20.4 cm^{-1}. Although the agreement is not quantitative, in both cases the shifts are qualitatively larger than the corresponding values for the nitrogen-bound complex. Given that these calculations do not include the effects of anharmonicity, we are satisfied with the agreement between theory and experiment. In part, owing to that fact that the line widths associated with the observed spectra are much broader than those of the nitrogen-bonded complex, the signal levels in the zero-field spectrum are quite low. Fortunately, the pendular spectrum could be used to optimize the signal levels. In particular, we found that the pendular spectrum optimized at the same zinc oven temperature and HCN pressure as used for the nitrogen-bound binary complex, giving further support to the assignment of this band to the hydrogen-bonded binary complex.

The low resolution of the zero-field spectrum would appear to prevent the determination of a rotational constant for this complex. However, since the rotational temperature can be assumed to be in equilibrium with the droplet temperature (0.37 K), the separation between the P and R branches can be used to estimate the rotational constant of this complex. The fitted spectrum shown in Figure 4 was generated using the line width determined from the pendular spectrum, using a linear rotor Hamiltonian. The resulting B rotational constant is given in Table 3. Although the uncertainty in this value is considerably larger than that for the nitrogen-bound complex (due to the lack of fine structure), it is still apparent that reduction in the rotational constant due to the helium is much greater than the usual factor of 3 (closer to 9) that has been observed for many other systems.[62] It is interesting to note that we observed the same anomaly for the hydrogen-bound Mg−HCN complex.[54] Indeed, it is clear from a large number of studies that the ratio of the gas phase and helium nanodroplet rotational constants depends on the details of the intermolecular potential between the solute molecule and the helium, which have not been calculated for the HCN−Zn binary system.

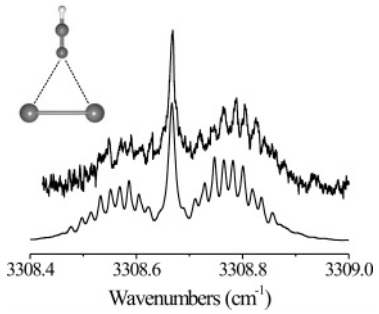

Figure 6. Partially resolved rovibrational spectrum of HCN−Zn_2. Although theory predicted a linear structure, the experimental spectrum is that of an asymmetric top.

HCN−Zn_2. We now turn our attention to the peak labeled 2 in Figure 2, which we have tentatively assigned to the HCN−Zn_2 complex. Here we note that the ECP/MP2 calculations gave the linear complex in Figure 1 as the only stable complex. We expected and did find a T-shaped geometry using ECP/MP2 methods, but upon harmonic vibration calculations, the structure returned a single imaginary frequency, indicating that the T-shaped structure was a transition state. This conclusion is clearly in poor agreement with the experimental data, displayed in Figure 6, which shows the spectrum of an asymmetric top (notice the Q branch). As a double check, a series of all-electron calculations [6-31+G(d) basis set for zinc and 6-311++G(d,p) for HCN] was performed, revealing both a linear and T-shaped isomer (with all real frequencies), the latter being the most stable. As stated above, Figure 6 immediately suggests that that the complex observed in the experiment is T-shaped, given the presence of the strong Q branch. In fact, the fit shown just below the experimental spectrum in Figure 6 was obtained by first using the rotational constants given by the calculations for the T-shaped structure (divided by 2.5) and then by fine-tuning the rotational constants to get the best agreement with experiment. The resulting rotational constants and vibrational band origin are given in Table 3. Although considerable effort was expended in searching for a linear isomer of the HCN−Zn_2 complex, no such features were observed in the spectrum. At this point we are uncertain as to whether this means the all-electron calculations are in error (perhaps due to the minimal basis sets) or if the barrier between the two isomers is simply too small to support the linear complex.

The Stark spectrum of the HCN−Zn_2 complex is given in Figure 7. A direct comparison of the experimental (3.7 D) and theoretical dipole moment was problematic for reasons stated above. Does one compare the experiment with ECP/MP2 calculations that give an imaginary frequency or does one compare it with all-electron calculations that utilize inferior basis sets? We chose to use the T-shaped geometry calculated via ECP/MP2 methods that contained a single imaginary frequency (11 cm^{-1}). This was done primarily because the HCN−Zn_2 complex is bound by weak van der Waals forces and large polarizable basis sets are required to reproduce the dipole induced dipole interactions that dominate the intermolecular forces. Table 2 gives the dipole moments of both the T-shaped

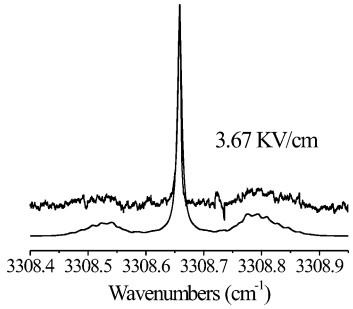

Figure 7. The Stark spectrum of HCN−Zn_2 recorded at 3.67 kV/cm using the T-shaped rotational constants determined from the field-free spectrum.

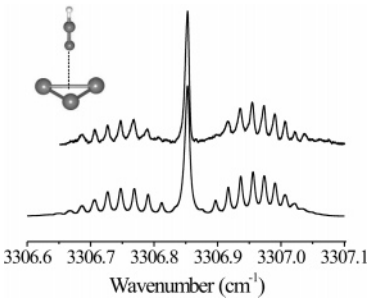

Figure 8. The fully resolved rovibrational spectrum of HCN−Zn_3. The symmetric top spectrum can only be due to the C_{3v} structure shown in the inset. The simulated spectrum was initially generated with a linear rotor Hamiltonian to fit the P and R structure. The *A* constant was obtained by fitting the relative intensities.

and linear isomers of the calculated HCN−Zn_2 structures, which are very close to each other. Due to the uncertainty involved in fitting the asymmetric top Stark spectrum and the uncertainty in the calculated dipole moments, we are forced to concede that the measurement of the dipole moment of HCN−Zn_2 gives no help determining the correct calculated structure, and we must rely solely on the measured field-free asymmetric top spectrum.

HCN−Zn_3. A zero-field spectrum for the HCN−Zn_3 complex is shown in Figure 8. This well-resolved spectrum appears to be that of a symmetric top complex, consistent with the ab initio structure shown in Figure 1. From the relatively small red-shift (relative to that expected for hydrogen-bound structures, namely, >25 cm^{-1}), we conclude that the HCN−Zn_3 complex has C_{3v} symmetry, with the nitrogen of HCN pointing toward the center of the zinc trimer. The calculated spectrum (lower spectrum) in Figure 8 was generated using the rotational constants and vibrational band origin given in Table 3. Determining the *A* rotational constant from a parallel band is always problematic, given that K is conserved in all of the observed transitions. As a result, we were able to use the relative intensities of the P, Q, and R branches (knowing the rotational temperature) to estimate *A*. Nevertheless, this estimate was also complicated by the fact that the broadening in the spectrum is dependent upon the rotational states in question, the lower J state transitions again being broader than those associated with higher J. As a result, the uncertainty in the *A* rotational constant is considerably larger than that for *B*. The corresponding ab initio data are given in Tables 2 and 3 and are in good agreement with experimental data. Indeed, the ratio of the ab initio (gas phase) (0.0278 cm^{-1}) to helium droplet (0.0107 cm^{-1}) *B* rotational constant is 2.6.

Figure 9 shows one of several Stark spectra recorded for the HCN−Zn_3 complex. The dipole moment obtained from fitting a number of such spectra (and used to generate the calculated spectrum shown in Figure 9) is 3.8 ± 0.1 D. Once again, this is slightly smaller than the ab initio value (3.97 D), consistent

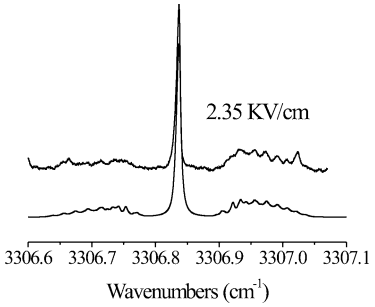

Figure 9. The Stark and simulated (below) spectrum of HCN−Zn_3 recorded at 2.35 kV/cm.

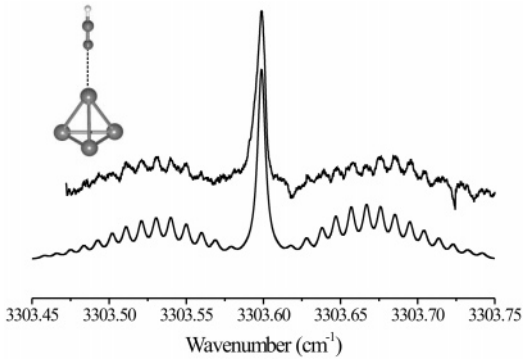

Figure 10. The rovibrational spectrum of the HCN−Zn_4 complex. Poor signal-to-noise prevented the precise measurement of dipole moment through Stark spectroscopy. The symmetric top simulated spectrum is given below the experimental one and is consisted with the proposed structure shown.

with the smaller complexes. Once again, all of the dipole moments quoted here have been corrected for the small effect of the helium solvent polarization.[53] It is interesting to note the trend of increasing dipole moment with increasing cluster size in both the experimental and ab initio results. This incremental increase is consistent with simple induction, given that the polarizability of the zinc cluster increases with size.

HCN−Zn_4. On the basis of our previous HCN−Mg_n work,[12] where the largest clusters were optimized with the highest oven temperatures and largest droplet sizes, the spectrum shown in Figure 10 was assigned to HCN−Zn_4. This trend is clearly shown in Figure 2, where the pendular spectrum is weighted toward the largest clusters at an oven temperature of 405 °C and nozzle temperature of 17.5 K. Turning our attention to the symmetry of the field-free spectrum shown in Figure 10, it is clear that this is due to the parallel band of a symmetric top. Assuming that this complex is due to a single HCN molecule bound to a Zn_4 cluster, only four possible geometries can exist that give rise to the symmetric top spectrum shown in the figure. The first two possible geometries are the HCN molecule bound to the 3-fold site of the Zn_4 tetrahedron, either H-end down or N-end down; the second two possible geometries are with the HCN bound to the on-top site of the tetrahedron, again, either N- or H-end down. Due to the relatively small frequency shift from HCN monomer and on the basis of our previous experience with weakly bound complexes, we can rule out the two hydrogen-bound species giving rise to the spectrum in Figure 10. For example, in the HCN−Zn results discussed above, a single zinc atom bound to the hydrogen side of HCN shifted the C−H stretch by 30.2 cm^{-1}. We are now left to consider the remaining two nitrogen-bound complexes.

The results of the our ab intio calculations for the HCN−Zn_4 complex are summarized in Tables 2 and 3, in addition to the structure shown in Figure 1. The structure that corresponds

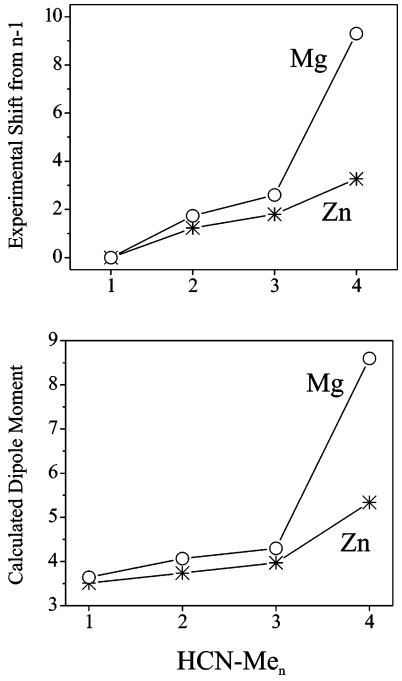

Figure 11. A comparison of the relative frequency shift (a) and calculated dipole moment (b) of HCN−Zn_n and HCN−Mg_n. Both plots illustrate the similarity for the $n \leq 3$ complexes and difference for the $n = 4$ complex.

to the nitrogen-end of the HCN molecule bound to the on-top site of the Zn_4 tetrahedron is the only possible structure to explain the spectrum shown in Figure 10. In fact, a test calculation of the HCN bound (N-end down) to the 3-fold site of the Zn_4 cluster was found to be totally repulsive, just as it was found in the case of HCN−Mg_4. Furthermore, there is excellent agreement between the experimental vibrational shift (7.6 cm^{-1}) and the calculated shift (7.80 cm^{-1}) from the HCN monomer.

The Stark spectra for HCN−Zn_4 have a very poor signal-to-noise ratio, and despite our best efforts, only limited dipole moment information was attainable. Through considerable experimental effort, we were able to determine an upper and lower limit of 6 and 4 D, respectively.

Discussion

Up to this point, we compared the individual HCN−Zn_n complexes with their corresponding counterparts in the previous HCN−Mg_n study. In the remainder of this paper, we will report the overall pattern similarities and differences between the two metal cluster−adsorbate systems. Let us begin by inspecting the overall frequency shift pattern of the HCN−Zn_n complexes. Figure 11 shows the plot of two different properties of HCN−Zn_n and HCN−Mg_n as a function of metal cluster size, namely, the experimental frequency shift from the $n - 1$ cluster, and the calculated dipole moment as a function of cluster size. The similarity in the frequency shift patterns is immediately apparent. The $n = 1-3$ clusters follow a pattern of increasing frequency shift with the addition of subsequent metal atoms. The larger frequency shift of the magnesium clusters are due to the larger polarizability of the magnesium atoms when compared to zinc. This behavior is well-known in weakly bound complexes and is explained by the increased interaction between the polarizable metal atom and the increased dipole moment of the vibrationally excited HCN molecule. In the previous HCN−Mg_n study we showed that the primary means of interaction between the HCN and magnesium clusters with $n = 1-3$ was a result of a dipole-induced polarization, i.e., physical bonds, whereas the HCN−Mg_4 began to show the signs of a dative bond through the transfer of charge from the lone pair on the nitrogen and to the atop site of the Mg_4 cluster.

The HCN−Zn_n clusters, while retaining the overall structure of the magnesium clusters, do not interact with the HCN as strongly. It appears that the HCN−Zn_4 complex follows a monotonic trend with increasing n. For example, as shown in Figure 11, the smooth increase in frequency shift and dipole moment for the HCN−Zn_n clusters is in sharp contrast to the large "jump" in frequency shift and dipole moment for the HCN−Mg_4 cluster. The mechanism for this weaker interaction lies primarily in the smaller polarizability of zinc (6.4 $Å^3$)[34] as compared to magnesium (10.6 $Å^3$),[34] but also can be traced to the more weakly bound nature of the bare zinc clusters themselves. For example, the extremely large dipole moment of HCN−Mg_4 (8.6 D) was attributed to the charge donation of the lone pair in HCN to the LUMO of the Mg_4 cluster, a LUMO that was the direct result of the increased hybridization of the 3s and 3p orbitals in magnesium. Indeed, this large degree of hybridization has been determined to be the cause of Mg_4's small bond length and large atomization energy when compared to the smaller clusters.[63]

Both magnesium and zinc have very similar electronic configurations and it is this connection that is at the heart of the overall similarity of the spectra presented here and previously.[12] Does the smaller dipole moment and smaller relative frequency shift of HCN−Zn_4 point to a smaller degree of hybridization of the 4s and 4p orbitals of zinc?

To investigate the difference between the HCN−Zn_n and HCN−Mg_n clusters, it is useful to first look to the bare clusters. First, let us examine the atomic spectroscopy data available for the two metals under discussion. Magnesium's lowest electronic transition ($3s3p \leftarrow 3s^2$) is 21 850 cm^{-1} [64] compared to zinc's ($4s4p \leftarrow 4s^2$), which is 32 311 cm^{-1}.[65] Already it is apparent that zinc must overcome a larger energy gap to hybridize with the first available empty orbital when compared to magnesium. The effect of this band gap has been addressed previously when comparing the small alkaline earth metal clusters.[63] In particular, Bauschlicher et al.[63] pointed out, in comparing Be_4, Mg_4, and Ca_4, that this gap is important in understanding the degree of *nsn*p hybridization and thus the relative bond energies of each alkaline earth metal cluster. However, Bauschlicher also pointed out that one could not disregard the effects of size in understanding the relative hybridization patterns in each cluster. For example, although Be and Mg have very similar atomic excitation energies ($2s2p \leftarrow 2s^2 = 21\,979$ cm^{-1} for beryllium and $3s2p \leftarrow 3s^2 = 21\,850$ cm^{-1} for magnesium), Be_4 is the more strongly bound than Mg_4, as well as having a greater degree of hybridization.[63] This difference in bonding strength is a result of the extremely diffuse nature of the 3p orbital relative to the 2p orbital in magnesium, so there is a larger energy "tax" to pay for the increased stabilization offered by hybridization.

We can now turn our attention back to the zinc and magnesium clusters. Table 4 displays the natural populations calculated at the MP2 level for both metal clusters. The populations support our previous conclusions, namely, for clusters of $n \leq 3$ in size there is little hybridization and are therefore predominately van der Waals in nature. Notice, however, that both metals increase their levels of p population in the $n = 4$ clusters. This is certainly no surprise for Mg_4, which has been calculated many times before,[63,66−70] but

TABLE 4: The Natural Populations for Zn_n and Mg_n, $n = 1-4$[a]

	4s	4p		3s	3p
Zn	1.95	0.05	Mg	1.95	0.05
Zn_2	1.95	0.06	Mg_2	1.94	0.05
Zn_3	1.93	0.07	Mg_3	1.88	0.1
Zn_4	1.83	0.16	Mg_4	1.75	0.21

[a] Both were calculated using the MP2 density. Calculations on Zn clusters used the ECP and associated valence basis set given in the text and Mg clusters used the 6-311++G(3df,3pd) basis set.

considering the much larger gap between the 4s and 4p orbitals in zinc, the degree to which the Zn_4 hybridizes seems anomalous. If, however, one considers the much smaller size of zinc due to its larger nuclear charge, it seems reasonable that zinc is able overcome its larger "energy penalty" for hybridization and form a relatively stable complex, just as Be_4 was calculated to be more stable than Mg_4.[63]

It is interesting to note that even though Zn_4 has a relatively large bond energy per atom and a relatively high degree of hybridization, the interaction with HCN is much less than what was observed in HCN−Mg_4. This is evident in the frequency shift data and the dipole moment data shown in Figure 11. Although our experiments were only able to provide an estimate of the dipole moment of HCN−Zn_4, the calculated dipole moment of 5.34 D is consistent with the weak interaction between HCN and Zn_4. It appears that the charge transfer that accounted for the large dipole moment in HCN−Mg_4 does not occur in HCN−Zn_4, and we can conclude that Zn_4 has a smaller electron affinity than Mg_4. Recently, this conclusion has been given further weight through private communication with Kit Bowen, whose work on the photoelectron spectroscopy of negatively charged Mg_n and Zn_n clusters has shown that singly charged Zn_4 anions are less stable than their anionic Mg_4 counterparts.[71]

Conclusions

The experimental vibrational shifts and bonding patterns of the HCN−Zn_n ($n = 1-4$) complexes are very similar to those determined for HCN−Mg_n ($n = 1-4$). The similarity between these two systems is primarily a result of the electronic configurations of magnesium and zinc. Both have closed s orbitals along with low-lying empty p orbitals. This characteristic is what determines the relatively small binding energies in all of these clusters and the fact that all bonds between the HCN and metal cluster are van der Waals in nature.

The differences between the HCN−Zn_n and HCN−Mg_n clusters are due to the differences in the polarizability of zinc and magnesium. The smaller polarizability results in a weaker dipole induced polarization of the zinc clusters and therefore a smaller vibrational red-shift. Although we were unable to acquire a precise dipole moment measurement for HCN−Zn_4, the calculated dipole moment was significantly smaller than that of the HCN−Mg_4 complex, indicating little or no charge transfer from the lone pair on the nitrogen in HCN to the LUMO of the Zn_4 cluster. This is most likely a result of zinc's energy gap between the filled 4s valence orbital and the empty 4p orbital, which is larger than the gap between the 3s and 3p orbitals in magnesium. The larger gap results in Zn_4's LUMO having less p character, which in turn makes Zn_4 a weaker electron acceptor than Mg_4.

Acknowledgment. This work was supported by the NSF (CHE-0446594).

References and Notes

(1) Busani, R.; Folkers, M.; Cheshnovsky, O. *Phys. Rev. Lett.* **1998**, *81*, 3836−3839.
(2) Kaiser, B.; Rademann, K. *Phys. Rev. Lett.* **1992**, *69*, 3204−3207.
(3) Brechignac, C.; Broyer, M.; Cahuzac, Ph.; Delacretaz, G.; Labastie, P.; Wolf, J. P.; Woste, L. *Phys. Rev. Lett.* **1988**, *60*, 275.
(4) Pastor, G. M.; Stampfli, P.; Bennemann, K. H. *Europhys. Lett.* **1988**, *7*, 419−424.
(5) Garcia, M. E.; Pastor, G. M.; Bennemann, K. H. *Phys. Rev. Lett.* **1991**, *67*, 1142−1145.
(6) Ruppel, M.; Rademann, K. *Chem. Phys. Lett.* **1992**, *197*, 280−285.
(7) Yonezawa, F.; Tanikawa, H. *J. Non-Cryst. Solids* **1996**, *205−207*, 793−796.
(8) Flad, H. J.; Schautz, F.; Wang, Y.; Dolg, M.; Savin, A. *Eur. Phys. J. D* **1999**, *6*, 243−254.
(9) Yu, M.; Dolg, M. *Chem. Phys. Lett.* **1997**, *273*, 329−336.
(10) Wang, J.; Wang, G.; Zhao, J. *Phys. Rev. A* **2003**, *68*, 013201.
(11) *Clusters of Atoms and Molecules I*; Springer-Verlag: Berlin, 1995.
(12) Stiles, P. L.; Moore, D. T.; Miller, R. E. *J. Chem. Phys.* **2004**, *121*, 3130.
(13) Hartmann, M.; Miller, R. E.; Toennies, J. P.; Vilesov, A. F. *Phys. Rev. Lett.* **1995**, *75*, 1566−1569.
(14) Hartmann, M.; Miller, R. E.; Toennies, J. P.; Vilesov, A. F. *Science* **1996**, *272*, 1631−1634.
(15) Kwon, Y.; Whaley, K. B. *J. Chem. Phys.* **2003**, *119*, 1986−1995.
(16) Paesani, F.; Whaley, K. B. *J. Chem. Phys.* **2004**, *121*, 4180−4192.
(17) Lehmann, K. K.; Callegari, C. *J. Chem. Phys.* **2002**, *117*, 1595−1603.
(18) Callegari, C.; Lehmann, K. K.; Schmied, R.; Scoles, G. *J. Chem. Phys.* **2001**, *115*, 10090−10110.
(19) Kaplan, I. G. *Int. J. Quantum Chem.* **1999**, *74*, 241−247.
(20) Kaplan, I. G.; Roszak, S.; Leszczynski, J. *Adv. Quantum. Chem.* **2001**, *40*, 257−278.
(21) Pyykko, P. *Chem. Rev.* **1988**, *88*, 563.
(22) Dolg, M.; Wedig, U.; Stoll, H.; Preuss, H. *J. Chem. Phys.* **1987**, *86*, 866−872.
(23) Müller, W.; Flesch, J.; Meyer, W. *J. Chem. Phys.* **1984**, *80*, 3297.
(24) Werner, H. J.; Knowles, P. J.; Amos, R. D.; Bernhardsson, A.; Berning, A.; Celani, P.; Cooper, D. L.; Deegan, M. J. O.; Dobbyn, A. J.; Eckert, F.; Hampel, C.; Hetzer, G.; Korona, T.; Lindh, R.; Lloyd, A. W.; McNicholas, S. J.; Manby, F. R.; Meyer, W.; Mura, M. E.; Nicklass, A.; Palmieri, P.; Pitzer, R.; Rauhut, G.; Schutz, M.; Schumann, U.; Stoll, H.; Stone, A. J.; Tarroni, R.; Thorsteinsson, T. *Molpro [2002.1];* University College Cardiff Consultants Limited: Wales, UK, 2002.
(25) Frisch, M. J.; Trucks, G. W.; Schlegel, H. B.; Scuseria, G. E.; Robb, M. A.; Cheeseman, J. R.; Montgomery, J. A., Jr.; Vreven, T.; Kudin, K. N.; Burant, J. C.; Millam, J. M.; Iyengar, S. S.; Tomasi, J.; Barone, V.; Mennucci, B.; Cossi, M.; Scalmani, G.; Rega, N.; Petersson, G. A.; Nakatsuji, H.; Hada, M.; Ehara, M.; Toyota, K.; Fukuda, R.; Hasegawa, J.; Ishida, M.; Nakajima, T.; Honda, Y.; Kitao, O.; Nakai, H.; Klene, M.; Li, X.; Knox, J. E.; Hratchian, H. P.; Cross, J. B.; Bakken, V.; Adamo, C.; Jaramillo, J.; Gomperts, R.; Stratmann, R. E.; Yazyev, O.; Austin, A. J.; Cammi, R.; Pomelli, C.; Ochterski, J. W.; Ayala, P. Y.; Morokuma, K.; Voth, G. A.; Salvador, P.; Dannenberg, J. J.; Zakrzewski, V. G.; Dapprich, S.; Daniels, A. D.; Strain, M. C.; Farkas, O.; Malick, D. K.; Rabuck, A. D.; Raghavachari, K.; Foresman, J. B.; Ortiz, J. V.; Cui, Q.; Baboul, A. G.; Clifford, S.; Cioslowski, J.; Stefanov, B. B.; Liu, G.; Liashenko, A.; Piskorz, P.; Komaromi, I.; Martin, R. L.; Fox, D. J.; Keith, T.; Al-Laham, M. A.; Peng, C. Y.; Nanayakkara, A.; Challacombe, M.; Gill, P. M. W.; Johnson, B.; Chen, W.; Wong, M. W.; Gonzalez, C.; Pople, J. A. *Gaussian 03*, revision A.1; Gaussian, Inc.: Pittsburgh, PA, 2003.
(26) Peterson, K. A.; Figgen, D.; Goll, E.; Stoll, H.; Dolg, M. *J. Chem. Phys.* **2003**, *119*, 11113−11123.
(27) Martin, J. M. L.; Sundermann, A. *J. Chem. Phys.* **2001**, *114*, 3408−3420.
(28) Schautz, F.; Flad, H. J.; Dolg, M. *Theor. Chem. Acc.* **1998**, *99*, 231−240.
(29) Nauta, K.; Moore, D. T.; Miller, R. E. *Faraday Discuss.* **1999**, *113*, 261−278.
(30) Nauta, K.; Miller, R. E. *J. Chem. Phys.* **1999**, *111*, 3426−3433.
(31) Nauta, K.; Miller, R. E. *J. Chem. Phys.* **2001**, *115*, 4508−4514.
(32) Lewerenz, M.; Schilling, B.; Toennies, J. P. *Chem. Phys. Lett.* **1993**, *206*, 381−387.
(33) Knuth E. L.; Schilling, B.; Toennies, J. P. *Proceedings of the 19th International Symposium on Rarefied Gas Dynamics*; 19 ed.; Oxford University Press: Oxford, UK, 1995; pp 270−276.
(34) *CRC Handbook of Chemistry and Physics*, 71 ed.; CRC Press: Boca Raton, FL, 1990.
(35) Cavallini, M.; Gallinaro, G.; Scoles, G. *Z. Naturforsch. A* **1967**, *22*, 413−414.

(36) Huang, Z. S.; Jucks, K. W.; Miller, R. E. *J. Chem. Phys.* **1986**, *85*, 3338−3341.
(37) Rost, J. M.; Griffin, J. C.; Friedrich, B.; Herschbach, D. R. *Phys. Rev. Lett.* **1992**, *68*, 1299−1301.
(38) Block, P. A.; Bohac, E. J.; Miller, R. E. *Phys. Rev. Lett.* **1992**, *68*, 1303−1306.
(39) Nauta, K.; Miller, R. E. *Phys. Rev. Lett.* **1999**, *82*, 4480−4483.
(40) Moore, D. T.; Oudejans, L.; Miller, R. E. *J. Chem. Phys.* **1999**, *110*, 197−208.
(41) Nauta, K.; Miller, R. E. *Science* **1999**, *283*, 1895−1897.
(42) Nauta, K.; Miller, R. E. *J. Chem. Phys.* **2001**, *115*, 10138−10145.
(43) Toennies, J. P.; Vilesov, A. F. *Angew. Chem. Int. Ed.* **2004**, *43*, 2622−2648.
(44) Lehmann, K. K. *Mol. Phys.* **1999**, *97*, 645−666.
(45) Lehmann, K. K.; Northby, J. A. *Mol. Phys.* **1999**, *97*, 639−644.
(46) Harms, J.; Toennies, J. P.; Dalfovo, F. *Phys. Rev. B* **1998**, *58*, 3341−3350.
(47) Reinhard, I.; Callegari, C.; Conjusteau, A.; Lehmann, K. K.; Scoles, G. *Phys. Rev. Lett.* **1999**, *82*, 5036−5039.
(48) Grebenev, S.; Havenith, M.; Madeja, F.; Toennies, J. P.; Vilesov, A. F. *J. Chem. Phys.* **2000**, *113*, 9060−9066.
(49) Conjusteau, A.; Callegari, C.; Reinhard, I.; Lehmann, K. K.; Scoles, G. *J. Chem. Phys.* **2000**, *113*, 4840−4843.
(50) Nauta, K.; Miller, R. E. *J. Chem. Phys.* **2001**, *115*, 8384−8392.
(51) Nauta, K.; Miller, R. E. *Chem. Phys. Lett.* **2001**, *350*, 225−232.
(52) Nauta, K.; Miller, R. E. *J. Chem. Phys.* **2000**, *113*, 9466−9469.
(53) Stiles, P. L.; Nauta, K.; Miller, R. E. *Phys. Rev. Lett.* **2003**, *90*, 135301.
(54) Stiles, P. L.; Moore, D. T.; Miller, R. E. *J. Chem. Phys.* **2003**, *118*, 7873−7881.
(55) Leopold, K. R.; Fraser, G. T.; Lin, F. J.; Nelson, D. D., Jr.; Klemperer, W. *J. Chem. Phys.* **1984**, *81*, 4922−4931.
(56) Drucker, S.; Tao, F. M.; Klemperer, W. *J. Phys. Chem.* **1995**, *99*, 2646−2655.
(57) Anderson, D. T.; Hinde, R. J.; Tam, S.; Fajardo, M. E. *J. Chem. Phys.* **2002**, *116*, 594−607.
(58) Carter, S.; Mills, I. M.; Handy, N. C. *J. Chem. Phys.* **1992**, *97*, 1606−1607.
(59) Bondi, A. *J. Phys. Chem.* **1964**, *68*, 441−451.
(60) Douberly, G. E.; Miller, R. E. *J. Phys. Chem. B* **2003**, *107*, 4500−4507.
(61) Nauta, K.; Miller, R. E. *Science* **2000**, *287*, 293−295.
(62) Nauta, K.; Miller, R. E. *J. Chem. Phys.* **2001**, *115*, 10254−10260.
(63) Bauschlicher, C. W., Jr.; Bagus, P. S.; Cox, B. N. *J. Chem. Phys.* **1982**, *77*, 4032−4038.
(64) Martin, W. C.; Zalubar, R. *J. Phys. Chem. Ref. Data* **1980**, *9*, 1−58.
(65) Gullberg, D.; Litzen, U. *Phys. Scripta* **2000**, *61*, 652−656.
(66) Akola, J.; Rytkonen, K.; Manninen, M. *Eur. Phys. J. D* **2001**, *16*, 21−24.
(67) Bauschlicher, C. W.; Partridge, H. *Chem. Phys. Lett.* **1999**, *300*, 364−368.
(68) Delaly, P.; Ballone, P.; Buttet, J. *Phys. Rev. B* **1992**, *45*, 3838−3841.
(69) Gong, X. G.; Zheng, Q. Q.; He, Y. *Phys. Lett. A* **1993**, *181*, 459−464.
(70) Kohn, A.; Weigend, F.; Ahlrichs, R. *Phys. Chem. Chem. Phys.* **2001**, *3*, 711−719.
(71) Bowen, K. H., private communication.